Catalysis Today 287 (2017) 91–98

Contents lists available at ScienceDirect

Catalysis Today

journal homepage: www.elsevier.com/locate/cattod

Novel preparation of ZnS from $Zn_5(CO_3)_2(OH)_6$ by the hydro- or solvothermal method for H_2 production

Octavio Aguilar[a], Francisco Tzompantzi[a,*], Raúl Pérez-Hernández[b], Ricardo Gómez[a], Agileo Hernández-Gordillo[c,*,1]

[a] Depto. de Química, Área de Catálisis, Universidad Autónoma Metropolitana – Iztapalapa, Av. San Rafael Atlixco No. 189, 09340, D.F. México, Mexico
[b] Instituto Nacional de Investigaciones Nucleares, Carretera México-Toluca S/N La Marquesa, Ocoyoacac, Edo. México C.P. 52750, Mexico
[c] Instituto de Investigaciones en Materiales, Universidad Nacional Autónoma de México, Circuito Exterior SN, Ciudad Universitaria, Coyoacán, C.P. 04510, México D.F., Mexico

ARTICLE INFO

Article history:
Received 19 June 2016
Received in revised form 22 August 2016
Accepted 21 November 2016
Available online 22 December 2016

Keywords:
ZnS
Hydrozincite
Solvothermal
Mesoporous
H_2 production

ABSTRACT

Mesoporous nanostructured zinc sulfide was prepared by the hydro or solvothermal method using synthesized *Hydrozincite* as a novel zinc precursor. ZnS from annealing ZnO and zinc nitrate as zinc sources was also investigated. Synthesized *Hydrozincite*, ZnO and the ZnS samples were characterized by XRD, UV–vis diffuse reflectance spectroscopy and FTIR analysis. The morphology and textural properties of the ZnS materials were investigated by SEM and N_2 adsorption-desorption, respectively. The photocatalytic properties of the ZnS materials were evaluated in the photocatalytic production of H_2 using a methanol-water solution at pH 6 (natural) under UV light irradiation. For the unique active mesoporous ZnS, an additional chemical stability test varying the pH solution (acid or alkaline media) using four reaction cycles was carried out and selected spent ZnS was characterized. The photoactiviy of synthesized mesoporous ZnS from *Hydrozincite* by solvothermal method was discussed as a function of the presence of ethylenediamine linked to ZnS.

1. Introduction

Zinc sulfide is an attractive semiconductor material employed in many application sectors that include light emitting diodes (LEDs), solar cells, active sensors [1–5], photocatalytic energy generation with highly efficient photochemical conversion [6] and H_2 production from water [7,8]. ZnS has bandgap energy of 3.6 eV, and has been extensively used as an active photocatalyst owing to the negatively redox potential of its conduction band and its high energy conversion efficiency [6,9], however, its photocatalytic properties can be enhanced by controlling the crystallinity, morphology and specific surface area [2,10]. Most of these physicochemical properties are influenced mainly by the synthesis method [11], experimental conditions [12–14] and sulfur precursor [1,15].

ZnS can be obtained by using commonly either zinc nitrate or acetate as the metal salt precursors, although, its preparation from the metallic oxide (ZnO) has been also reported, obtaining best photocatalytic properties for H_2 production [16]. The synthesis of ZnS can be performed in a water solution or organic solvent (hydro/solvothermal method), obtaining nanostructured ZnS with different morphologies such as spheres or bulky structures [15], microspheres [1,17,18], flower microspheres [19], nanoplates [20], branched nanorods [21,22] and nanowires [23]. Specifically, by using ethanol as organic solvent, ZnS flower-microstructures [3] or mesoporous materials with high specific surface area [2] can be obtained.

On the other hand, zinc hydroxyl carbonate [$Zn_5(CO_3)_2(OH)_6$], commonly known as *Hydrozincite*, has been used as zinc source to obtain ZnO by annealing, achieving a material with high porosity (nanoporous materials) [24–29]. As far as we know, *Hydrozincite* has never been used directly as Zn source for the preparation of ZnS. Thus, in this work, the photocatalytic properties of prepared mesoporous nanostructured ZnS by hydro- or solvothermal method (in water or ethanol, respectively) using *Hydrozincite* as a novel zinc precursor was investigated. For comparison, nanostructured ZnS was also prepared from either ZnO or zinc nitrate. *Hydrozincite* was obtained by a simple precipitation method, and ZnO was obtained

* Corresponding authors.
E-mail addresses: fjtz@xanum.uam.mx (F. Tzompantzi), agileo12@hotmail.com, agileohg@iim.unam.mx (A. Hernández-Gordillo).
[1] CONACYT Research Fellow.

http://dx.doi.org/10.1016/j.cattod.2016.11.042
0920-5861/

Table 1
Data of synthesis condition, proportion phase, bandgap energy and specific surface area of synthesized ZnS materials.

Nombre	Thermal Method	Zinc Source	Proportion Hexagonal (%)	E_g (eV)	S_g ($m^2\ g^{-1}$)
H-ZO	Hydro	ZnO	5	3.43	91
H-HZn	Hydro	*Hydrozincite*	5	3.39	96
S-HZn	Solvo	*Hydrozincite*	0	3.51	160
S-ZN	Solvo	Zn-$(NO_3)_2$	5	3.45	91

Eg = Band gap energy, Sg = Specific surface area.

by annealing *Hydrozincite*. All the nanostructured ZnS samples were characterized by XRD, FTIR, UV–vis diffuse reflectance spectroscopy and nitrogen physisorption. Finally, the select mesoporous ZnS from *Hydrozincite* precursor was evaluated in the photocatalytic production of H_2 using a methanol-water solution under UV light irradiation, varying the photocatalyst load and varying the pH solution during the reaction cycles.

2. Methodology

2.1. Synthesis of hydrozincite and ZnO

In a glass flask containing water, a suitable amount of a zinc nitrate [$Zn(NO_3)_2{\cdot}6H_2O$] salt (J.T. Baker 99.6% purity) was dissolved in deionized water at room temperature, and subsequently, an appropriate amount of urea (Reasol, 99%) was added (molar ratio Zn:urea of 1:3). Then, the homogenous solution was heated up to boiling point (~94 °C) under vigorous stirring and refluxed for 36 h. During the hydrolysis of urea for the carbonation process, the resultant solution pH was 8. The precipitated solid was several times washed with hot water and after, it was dried at 90 °C all night long. The as-dried solid was pulverized and labeled as ***Hzn*** sample; then, an appropriate amount of the *Hydrozincite* solid was annealed at 400 °C for 5 h to obtain ZnO.

2.2. Synthesis of nanostructured ZnS

In a glass flask containing deionized water, an appropriate amount of a zinc source, annealed ZnO or synthesized *Hydrozincite*, was dissolved; subsequently, thiourea (Reasol ≥ 99% purity) was added as sulfur source, maintaining a molar ratio of Zn:S of 1:1. The aqueous solution mixture, containing either ZnO or *Hydrozincite*, was sonicated for 3 h and after, the pH was adjusted to 11–12 by adding ethylenediamine; finally, the solution was poured into a Parr reactor, reaching a temperature of 140 °C for 10 h (hydrothermal method). The synthesized ZnS was washed several times with ethanol-water and dried at 90 °C for 24 h.

For comparison purposes, nanostructured ZnS was also obtained in ethanol (Sigma-Aldrich HPLC grade) by solvothermal method under the same conditions mentioned above, using a $Zn(NO_3)_2{\cdot}6H_2O$ salt or synthesized *Hydrozincite* as zinc sources. The ZnS samples prepared by the hydrothermal method were labeled as **H-X** and those prepared by the solvothermal method as **S-X**, where X represents the zinc Source: ZO for ZnO, HZn for Hydrozincite and ZN for zinc nitrate (Table 1).

2.3. Characterization of ZnS materials

The as-synthesized materials were characterized by X-Ray diffraction (XRD) using a Bruker D2 Phaser diffractometer with Cu-K∞ radiation. The XRD patterns were recorded in a 2θ scanning range of 5 to 80°, using a step of 0.01° and a counting time of 0.6 s per step. The thermogravimetric analysis (TGA) was performed using a STA 1000 simultaneous thermal analyzer at a heating rate of 10 °C/min with air flow of 10 mL/s.

The characteristic vibrations of the materials were determined by using a FTIR Affinity-1 Shimadzu spectrophotometer equipped with an attenuate total reflectance ATR accessory.

The UV–vis diffuse reflectance spectra were obtained from a Cary-100 spectrophotometer equipped with an integrating sphere. Barium sulfate was used as reference. Photoluminescence emission of the materials was recorded on a SCINCO fluorescence spectrometer FS-2 from 500 to 800 nm, using an excitation wavelength of 254 nm. N_2 adsorption-desorption isotherms were obtained employing a Quantachrome Autosorb-3B equipment. Before analysis, the samples were degassed at 130° C for 24 h. The specific area was calculated from the BET method.

2.4. Photocatalytic H_2 production

The photocatalytic evaluation of materials was carried out in a batch-glass-home-made cylindrical reactor: diameter of 5.5 cm and volume of 270 mL [30]. A quartz tube was placed inside the reactor with a mercury lamp (Pen-Ray), which emits light with a wavelength of 254 nm, 2.16 W of power and 2.2 $mWcm^{-2}$ of intensity. In each reaction, 100 mg of catalyst and 200 mL of a MetOH-water solution (1:1 volume ratio) was used. Before each reaction, the system was purged with N_2 for 10 min in order to remove O_2 and H_2 present in the system. Throughout irradiation, the reaction system was kept under magnetic stirring at room temperature in order to maintain good dispersion of the catalyst in the MetOH-water solution. The amount of produced H_2 was determined using a previously made calibration curve and it was quantified every hour by employing a gas chromatograph equipped with TCD detector, Shin-carbon column and N_2 used as carrier.

Additional test were carried out varying the photocatalyst load (25, 50 and 100 mg) at pH 6 (natural) with the active ZnS. Cycles of H_2 production reaction were run to select the best ZnS, using the same irradiated MeTOH-H_2O solution at different pH solution (4.5, 6.0 and 9.8) adjusted by adding HNO_3 or NaOH. Before each reaction cycle, the system was purged with N_2 for 10 min in order to remove O_2 and H_2 present in the system and the UV-lamp was turned on again for the 4 cycles. At the end of the reaction, the spent ZnS was recovered and characterized after the forth reaction cycles at pH 6.

3. Results and discussion

3.1. Characterization of hydrozincite and ZnO

The thermogravimetric (TG) analysis of the synthesized **HZn** sample (Fig. 1A) showed a strong weight loss (~22 wt.%) in the temperature interval from 150 to 260 °C, which is associated with dehydroxylation (—OH) and decarbonation ($—CO_3$) due to the decomposition of the zinc hydroxyl carbonate precursor to ZnO [28,31]. Afterwards, a slight weight loss (~1 wt.%) was observed up to 400 °C, which is probably due to residual elimination. The total weight loss (~23 wt.%) is close to the calculated theoretical value for *Hydrozincite* transformation to ZnO. The X-ray diffraction pattern for the **HZn** sample (Fig. 1B) exhibits peaks that correspond to monoclinic *Hydrozincite* ($Zn_5(CO_3)_2(OH)_6$), which is indexed

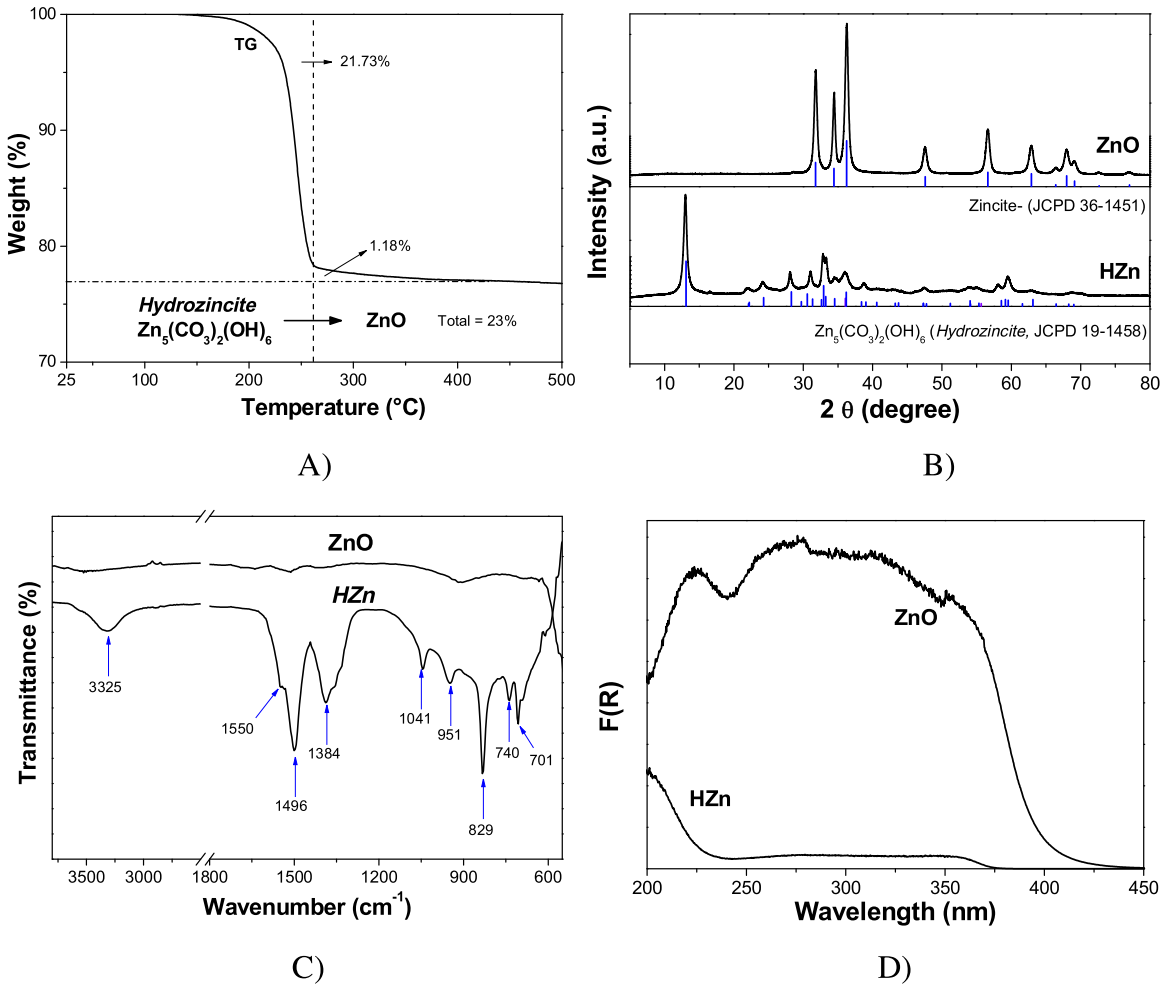

Fig. 1. A) TG analysis of as-synthesized **HZn** sample, B) X-ray diffraction patterns, C) FTIR analysis and D) Diffuse reflectance spectra of as-synthesized **HZn** and annealed ZnO sample.

from the JCPDS No. 19-1458. After, *Hydrozincite* was annealed at 400 °C, exhibiting peaks corresponding to the hexagonal structure of the zincite phase of ZnO, indexed from the JCPDS No. 36-1451 [24,26,31]. No other peaks related to impurities such as zinc carbonate and zinc hydroxide were observed. The intense narrow peaks indicate that the annealed ZnO is well crystallized. The FTIR analysis for the **HZn** sample (Fig. 1C) exhibits a peak at 3325 cm^{-1}, assigned to stretching vibrations of O—H groups that may come from a small quantity of adsorbed H_2O molecules on the sample. The main vibration bands at 1550–1496 and 1384 cm^{-1} are assigned to different carbonate species. The signal at 1550–1496 cm^{-1} is attributed to the adsorption of free CO_3^{2-} species or to antisymmetric O—C—O stretching vibrations. These free CO_3^{2-} species have also been associated with vibration bands at around 1041, 829 and 740–701 cm^{-1}, which correspond to the $\upsilon 1$ symmetry, $\upsilon 2$ out-of-plane mode and $\upsilon 4$ in-plane mode, respectively, which are characteristic of the $Zn_5(CO_3)_2(OH)_6$ precursor [31]. The signal at 1384 cm^{-1} is assigned to symmetric O—C—O stretching vibrations ($\upsilon 3$ mode) of monodentated carbonate (CO_3^{2-}) species in the structure [32]. The diffuse reflectance spectra of *Hydrozincite* (Fig. 1D) shows an absorption edge at high energy from 210 to 190 nm, which is associated with low electronic transitions [32] whereas ZnO exhibits an absorption edge from 390 to 370 nm, corresponding to an electron transition from the valence band to the conduction band of ZnO [32,33]. The specific surface areas of *Hydrozincite* and ZnO are 28 and 44 m^2/g, respectively.

3.2. Characterization of nanostructured ZnS

The X-ray diffraction patterns of the ZnS samples prepared from either *Hydrozincite* or ZnO by the hydrothermal method (Fig. 2A) show mainly diffraction peaks that correspond to the cubic structure of the sphalerite phase of ZnS (JCPDS No. 01-0792)[9,34], however, small diffraction peaks indicating the presence of the hexagonal structure of the wurtzite phase of ZnS were also detected (JCPDS Card No. 36-1450) [16]. The intensity of the diffraction peaks is fairly strong and broad, indicating that it is highly crystalline on the nanometric scale [13].

For the ZnS samples prepared from either a zinc nitrate salt or *Hydrozincite* by the solvothermal method, different crystalline structures were observed (Fig. 2A). Using a zinc nitrate salt, two ZnS phases corresponding to the cubic-sphalerite and hexagonal-wurtzite phases were detected, where sphalerite is the predominant phase (Table 1). The formation of two crystalline ZnS phases has been typically reported when a zinc nitrate salt is used [3]. On the other hand, when *Hydrozincite* was used, only a single sphalerite-phase of ZnS was obtained. In addition, the broadening diffraction peaks indicate nanocrystalline materials. In all the cases, the diffraction peaks of the zinc source were not detected, suggesting that *Hydrozincite* and ZnO were fully sulphided. The proportion of each phase was calculated by applying the Halder-Wagner method, and the data area shown in Table 1. The proportion of the hexagonal phase is very low (<5%).

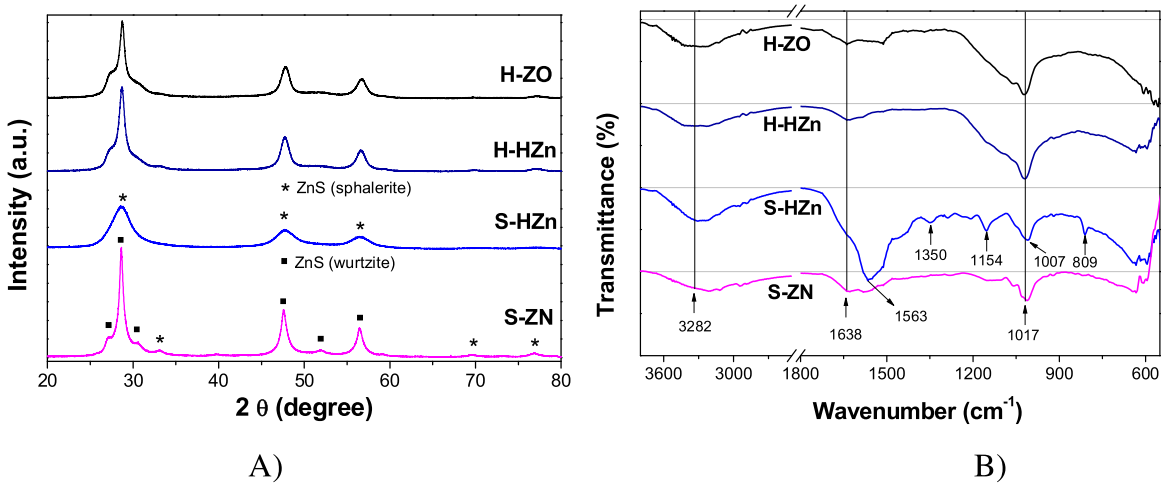

Fig. 2. A) X-ray diffraction patterns and B) FTIR analysis of ZnS samples prepared by hydro- and solvothermal method.

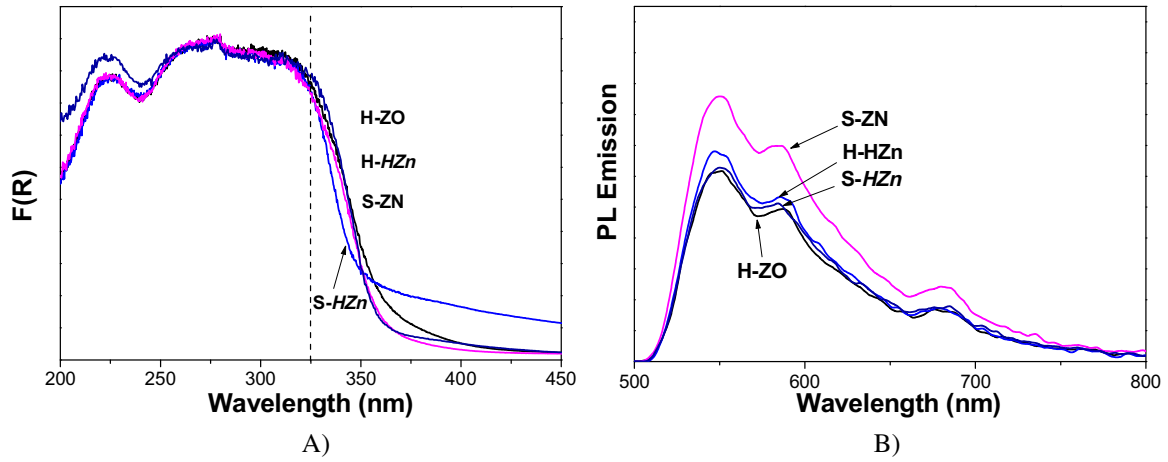

Fig. 3. A) Diffuse reflectance spectra and B) Photoluminescence of ZnS samples prepared by hydro- and solvothermal method.

The FTIR analysis of all the ZnS samples (Fig. 2B) exhibited vibration peaks at 3282 cm^{-1}, which can be assigned to stretching vibrations of O—H groups that may come from a small quantity of H_2O adsorbed on the sample. The peaks at 1638 cm^{-1} correspond to the C=O stretching modes caused by the absorption of CO_2 on the ZnS surface [35]. Not with standing, for the **S-HZn** sample, additional vibration bands at 1563, 1350, 1154, 1007 and 809 cm^{-1} are exhibited, suggesting the presence of additional compounds on the ZnS surface. These peaks have been associated with the stretching vibrations of C—H, —NH_2, and C—N bonds, respectively, of ethylenediamine, which are originated from the $M(EN)^{2+}$ complex, where the ethylenediamine molecule is linked to superficial Zn^{2+} ions on the ZnS surface [30]. All the ZnS samples exhibited vibration peaks at around 1017 and 630 cm^{-1}, which are attributed to ZnS bands corresponding to sulfides [14,35]. No peaks of the zinc source were detected.

UV–vis diffuse reflectance spectra of the ZnS samples (Fig. 3A) show almost the same absorption edge from 360 to 330 nm. This absorption edge is associated with electron transitions from the valence band to the conduction band of ZnS [3]. The bandgap energy of ZnS is close to 3.4 ± 0.1 eV (Table 1). In the case of the **S-HZn** sample, its absorption edge was slightly blue-shifted, probably due to the quantum size effect [36]. The bandgap energy is 3.5 eV and it showed absorption in the visible region (350–500 nm) assigned to the crystal or surface defects [30]. The surface defects might be generated when the ethylenediamine molecule is linked to superficial Zn^{2+} ions. The photoluminescence spectra of ZnS samples (Fig. 3B) exhibit an intense green emission peak at around 570 nm, which corresponds to the recombination of electrons from the energy level of sulfur vacancies with the holes from the energy level of zinc vacancies; this PL emission at 510–570 nm has been also associated with elemental S species on the surface of ZnS particles [15,17].

SEM images of the synthesized ZnS samples (Fig. 4) show slight differences in their morphology. By the hydrothermal method using ZnO, ZnS exhibited large particles, which are composed of many small nanoparticles of diverse dimensions (10–300 nm); in contrast, by using *Hydrozincite*, nanoparticles and enlarged ZnS particles with dimensions between 500 nm and 1 μm were observed. Both ZnS samples prepared by the solvothermal method exhibited nanoparticles between 100 and 500 nm, independently of the used zinc source.

The ZnS samples prepared by the hydrothermal method exhibited a N_2 adsorption-desorption isotherm of Type III (Fig. 5A) according to the IUPAC classification. On the other hand, for the ZnS prepared by the solvothermal method, a Type IV isotherm (Fig. 5B) is observed, which is characteristic of mesoporous materials. The specific surface area is between 91 and 160 m^2/g, being the ***S*-HZn** sample the one with the highest specific surface area (160 m^2/g). This result suggests that the solvothermal method using ethanol as solvent and either *Hydrozincite* or zinc nitrate as zinc sources could be an alternative to obtain mesoporous materials.

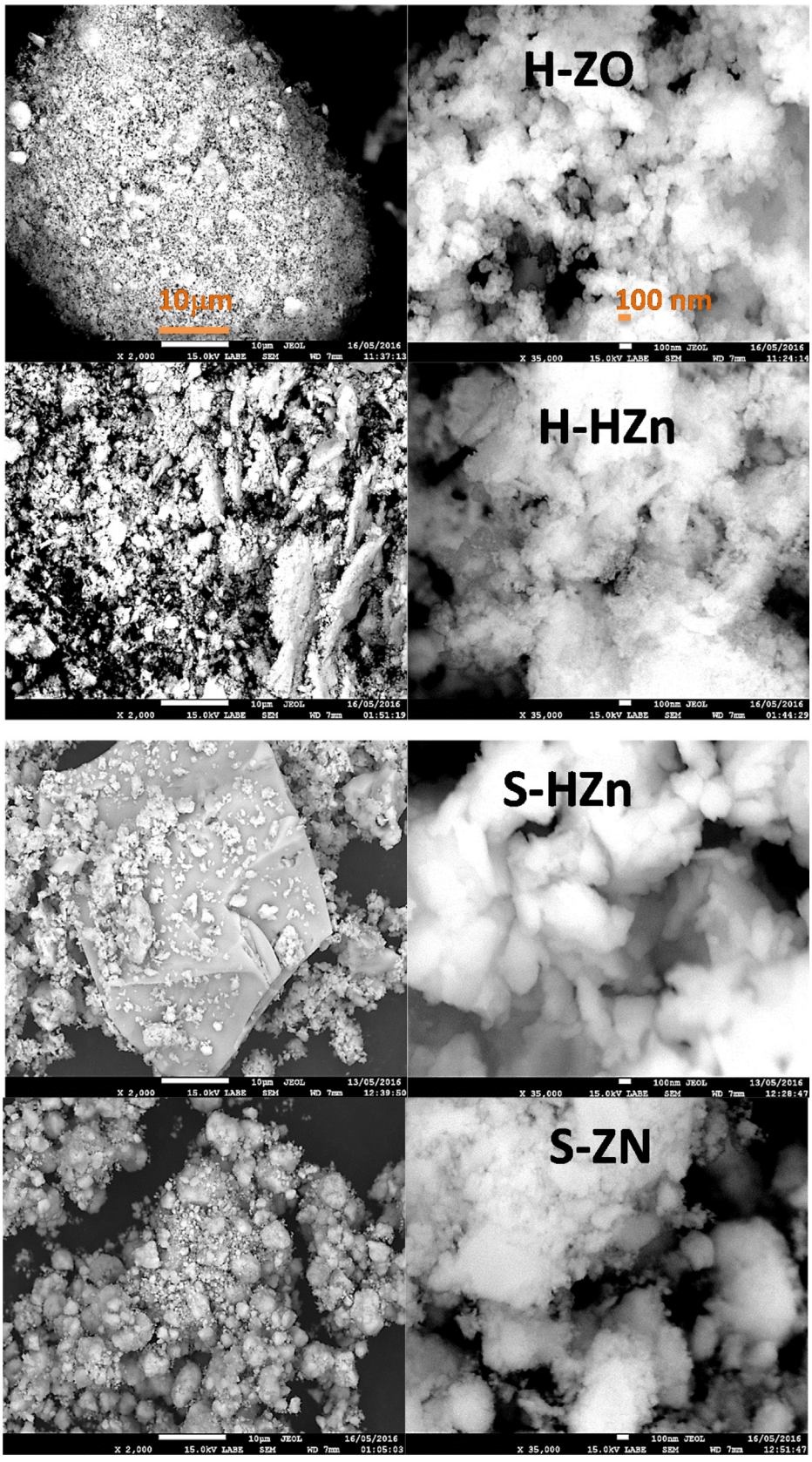

Fig. 4. SEM images for the synthesized ZnS samples by hydrothermal (**H-ZO** and **H-HZn**) and solvothermal method (**S-HZn** and **S-ZN**).

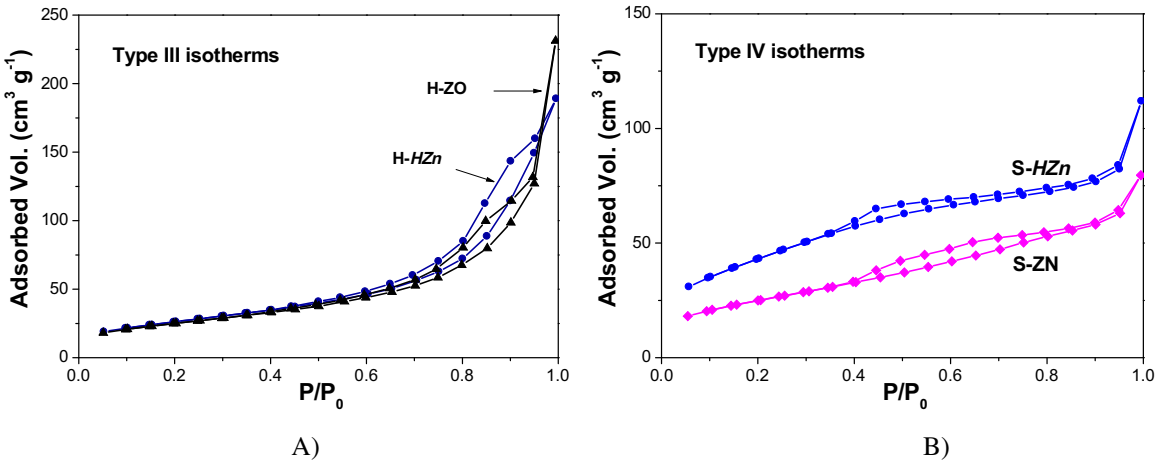

Fig. 5. Nitrogen physisorption of ZnS samples prepared by: A) hydro- and B) solvothermal method.

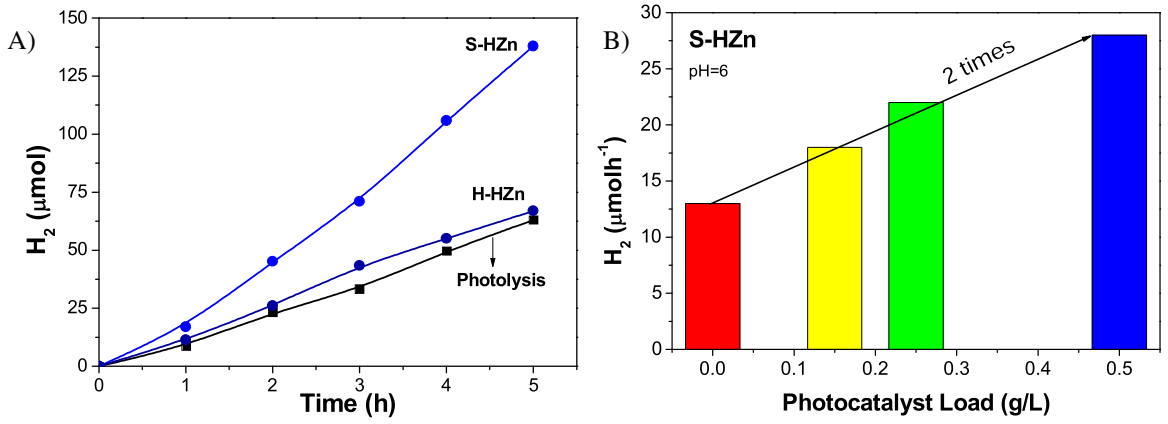

Fig. 6. Profile of H_2 production: A) as function of time for the photolysis and ZnS samples and B) as a function of photocatalyst load using **S-HZn** sample at pH 6.

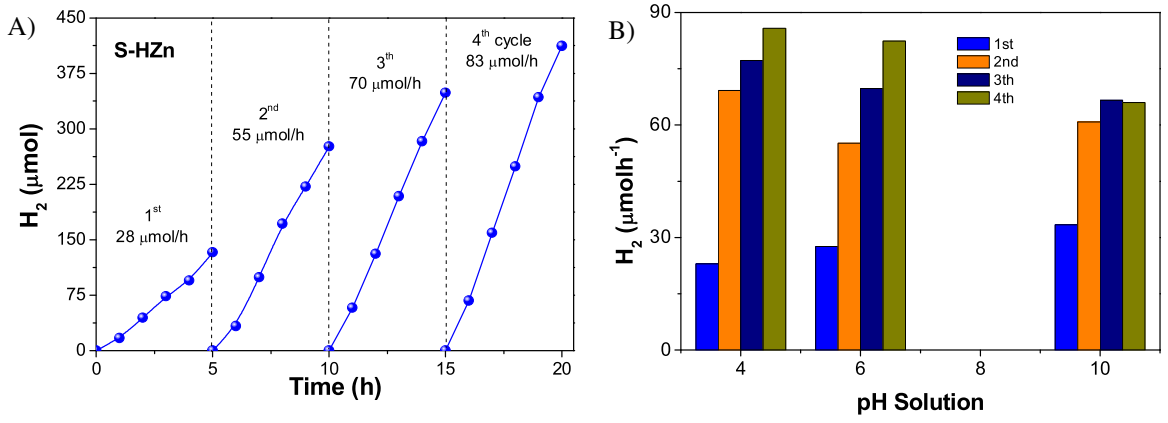

Fig. 7. Profile of H_2 production: A) at different reaction cycles at pH 6 B) at different pH = 4.8, 6.5 or 10.2, using **S-HZn** sample.

3.3. *Photocatalytic test and cycles for H_2 production*

The H_2 production profile at pH 6 for the synthesized ZnS samples (Fig. 6A) shows that the produced H_2 was increased as time passed by, similarly to photolysis (without catalyst); this means that the photoactivity of the ZnS samples was negligible, except for the mesoporous ***S*-HZn** sample that showed a rate of 28 μmol/h of H_2. The effect of the photocatalyst load (Fig. 6B), showed a linear correlation between produced H_2 and the photocatalyst load which was 2.3 times higher than that of photolysis. For the rest of ZnS samples the increasing in the produced H_2 was not observed. Considering that the electronic properties of all the ZnS samples are similar, but the formation of a single cubic phase and the presence of sulfur vacancies (state defects) on the surface of the ***S*-HZn** sample, generated by the presence of ethylenediamine, could be the cause of the observed photoactivity, where these surface states act as electron traps that promote a better electron-hole pair separation and induce photocatalytic activity in the ZnS sample.

In addition, the photocatalytic activity of the ***S*-HZn** sample was enhanced after each reaction cycle at pH 6 (Fig. 7A), achieving a ~3

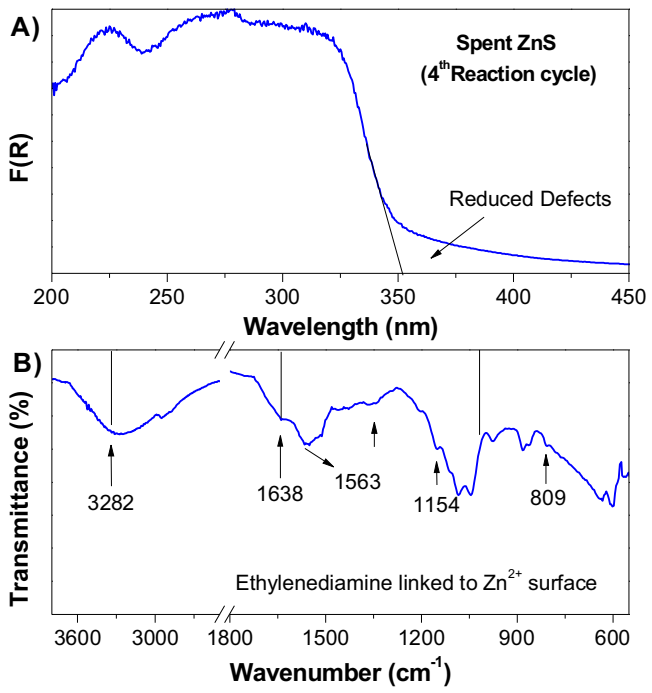

Fig. 8. A) UV–vis and B) FTIR analysis of the spent ZnS after the forth reaction cycle.

times higher H_2 production rate than that of the first reaction cycle, which is even ~7 times higher than that of photolysis. In acid media (pH 4.5) the profile of H_2 production rate during of the fourth reaction cycle was similar to than that at pH 6 (Fig. 7B), but in alkaline media (pH 9.8) the initial H_2 production rate was 33 μmol/h, then it was increased and remained ~2 times (66 μmol/h) after of the third reaction cycle. This suggests that the mesoporous ZnS is chemically stable to photocorrotion phenomena inclusive is chemically stable in acid media probably due to the presence of ethylenediamine on ZnS surface, inhibiting the photocorrotion effect by the inorganic acid. The presence of sulfur vacancies and formed intermediaries from irradiated methanol-water solution contributes to improve the H_2 evolution.

3.4. Characterization of spent ZnS (S-HZn sample)

After the 4th reaction cycle at pH 6, the crystalline structure of the spent, single-cubic phase of the ZnS photocatalyst showed no change (not shown); however, the electronic and surface properties were slightly modified. The diffuse reflectance spectra show the same intrinsic electronic transition of the spent ZnS after the forth reaction cycles, but the absorption edge in the visible region was decreased (Fig. 8A), suggesting that the crystal defects on ZnS decreased. This result is in agreement with the FTIR analysis (Fig. 8B), where the vibration bands of the C-H, $-NH_2$, and C-N bonds of ethylenediamine linked to Zn^{2+} on the ZnS surface were also slightly decreased. The characteristic vibration peaks of CO_2 adsorbed on the ZnS surface remain unaltered, however, new vibration bands appear in the intervals from 1150 to 1005 cm^{-1} assigned to the residual products of secondary reactions. The persistent ethylenediamine molecule linked to the ZnS surface suggests that it is responsible for generating active sites for photocatalytic activity.

4. Conclusion

Mesoporous, single-cubic-phase ZnS with high specific surface area was successfully synthesized by the solvothermal method using ethanol as solvent through the sulphidation of *Hydrozincite* with thiourea. The hydrothermal method, using either *Hydrozincite* or a ZnO precursor, and the solvothermal method, using zinc nitrate, induce the formation of a mixture of a crystalline-cubic-hexagonal phase. Using *Hydrozincite* as zinc precursor allows ethylenediamine to be linked to the mesoporous-cubic-ZnS surface, causing surface defects that generate surface states and, as consequence, a high electron-hole pair separation is achieved to carry out the H_2 production by several reaction cycles.

Acknowledgements

Octavio Aguilar thanks would like to thank CONACYT for a scholarship granted No. 269185. The authors would like to acknowledge the financial support provided by CONACyT (Project 154994) and CONACYT for the Cátedras-Conacyt/1169 project.

References

[1] M. Kaur, C.M. Nagaraja, Template-free synthesis of ZnS nanocrystals with a new sulfur source and their photocatalytic study, Mater. Lett. 154 (2015) 90–93.
[2] Y.-P. Zhu, J. Li, T.-Y. Ma, Y.-P. Liu, G. Du, Z.-Y. Yuan, Sonochemistry-assisted synthesis and optical properties of mesoporous ZnS nanomaterials, J. Mater. Chem. A 2 (2014) 1093–1101.
[3] W. Bai, L. Cai, C. Wu, X. Xiao, X. Fan, K. Chen, J. Lin, Alcohothermal synthesis of flower-like ZnS nano-microstructures with high visible light photocatalytic activity, Mater. Lett. 124 (2014) 177–180.
[4] X. Ye, Y. Li, J. Dong, J. Xiao, Y. Ma, L. Qi, Facile synthesis of ZnS nanobowl arrays and their applications as 2D photonic crystal sensors, J. Mater. Chem. C 1 (2013) 6112.
[5] B. Bochev, G. Yordanov, Room temperature synthesis of thioglycolate-coated zinc sulfide (ZnS) nanoparticles in aqueous medium and their physicochemical characterization, Coll. Surf. A 441 (2014) 84–90.
[6] B. Pal, B. Pal, Tuning the optical and photocatalytic properties of anisotropic ZnS nanostructures for the selective reduction of nitroaromatics, Chem. Eng. J. 263 (2015) 200–208.
[7] Z. Fang, S. Weng, X. Ye, W. Feng, Z. Zheng, M. Lu, S. Lin, X. Fu, P. Liu, Defect engineering and phase junction architecture of wide-bandgap ZnS for conflicting visible light activity in photocatalytic H(2) evolution, ACS Appl. Mater. Interfaces 7 (2015) 13915–13924.
[8] J. Zhang, Y. Wang, J. Zhang, Z. Lin, F. Huang, J. Yu, Enhanced photocatalytic hydrogen production activities of Au-loaded ZnS flowers, ACS Appl. Mater. Interfaces 5 (2013) 1031–1037.
[9] L. Yin, D. Wang, J. Huang, L. Cao, H. Ouyang, X. Yong, Morphology-controllable synthesis and enhanced photocatalytic activity of ZnS nanoparticles, J. Alloys Compd. 664 (2016) 476–480.
[10] Y. Tian, G.-F. Huang, L.-J. Tang, M.-G. Xia, W.-Q. Huang, Z.-L. Ma, Size-controllable synthesis and enhanced photocatalytic activity of porous ZnS nanospheres, Mater. Lett. 83 (2012) 104–107.
[11] S. Ummartyotin, Y. Infahsaeng, A comprehensive review on ZnS: From synthesis to an approach on solar cell, Renew. Sustain. Energy Rev. 55 (2016) 17–24.
[12] H.F. Qi, J.L. Li, Y. Shi, J.J. Xie, F. Lei, Low-temperature synthesis and photoluminescence properties of wurtzite three-dimensional ZnS nanostructures, Adv. Mater. Res. 1058 (2014) 65–68.
[13] L. Yin, D. Zhang, D. Wang, X. Kong, J. Huang, F. Wang, Y. Wu, Size dependent photocatalytic activity of ZnS nanostructures prepared by a facile precipitation method, Mater. Sci. Eng. B 208 (2016) 15–21.
[14] X. Tian, J. Wen, S. Wang, J. Hu, J. Li, H. Peng, Starch-assisted synthesis and optical properties of ZnS nanoparticles, Mater. Res. Bull. 77 (2016) 279–283.
[15] Q. Ma, Y. Wang, J. Kong, H. Jia, Tunable synthesis, characterization and photocatalytic properties of various ZnS nanostructures, Ceram. Int. 42 (2016) 2854–2860.
[16] N. Jiang, R. Wu, J. Li, Y.F. Sun, J.K. Jian, Ethanol amine-assisted solvothermal growth of wurtzite-structured ZnS thin nanorods, J. Alloys Compd. 536 (2012) 85–90.
[17] M. Li, F. Wang, Z. Wang, M. Zubair Iqbal, Q.-U.-A. Javed, Y. Lu, M. Xu, Q. Li, Synthesis of complex 3D ZnS architectures via a template-free solvothermal approach and the optical properties, Mater. Lett. 112 (2013) 72–74.
[18] A.K. Shahi, B.K. Pandey, R. Gopal, PEG mediated solvothermal synthesis of fine ZnS sub-micro and microspheres and their optical properties, Mater. Lett. 116 (2014) 112–115.
[19] M. Li, F. Wang, Z. Wang, M. Zubair Iqbal, Q.-U.-A. Javed, Y. Lu, M. Xu, Q. Li, Solvothermal preparation of flower-like ZnS microspheres, their photoluminescence and hydrogen absorption characteristics, Mater. Lett. 112 (2013) 81–83.
[20] M. Shakouri-Arani, M. Salavati-Niasari, Synthesis and characterization of wurtzite ZnS nanoplates through simple solvothermal method with a novel approach, J. Ind. Eng. Chem. 20 (2014) 3179–3185.

[21] H. Wang, Z. Chen, Q. Cheng, L. Yuan, Solvothermal synthesis and optical properties of single-crystal ZnS nanorods, J. Alloys Compd. 478 (2009) 872–875.
[22] L. Chai, W. He, L. Sun, F. Jin, X. Hu, J. Ma, Solvothermal synthesis of wurtzite ZnS complex spheres with high hierarchy, Mater. Lett. 120 (2014) 26–29.
[23] W.-H. Zhang, W.-D. Zhang, One-pot solvothermal strategy for the synthesis of ultrathin ZnS nanowires, Mater. Lett. 98 (2013) 5–7.
[24] K. Zhou, Q. Zhang, Y. Shi, S. Jiang, Y. Hu, Z. Gui, A facile method for preparation ZnO with different morphology and their optical property, J. Alloys Compd. 577 (2013) 389–394.
[25] J.A. Paramo, Y.M. Strzhemechny, T. Endo, Z. Crnjak Orel, Correlation of defect-related optoelectronic properties in Zn5(OH)6(CO3)2/ZnO nanostructures with their quasi-fractal dimensionality, J. Nanomater. 2015 (2015) 1–6.
[26] F. Fan, P. Tang, Y. Wang, Y. Feng, A. Chen, R. Luo, D. Li, Facile synthesis and gas sensing properties of tubular hierarchical ZnO self-assembled by porous nanosheets, Sens. Actuators B 215 (2015) 231–240.
[27] F. Meng, S. Ge, Y. Jia, B. Sun, Y. Sun, C. Wang, H. Wu, Z. Jin, M. Li, Interlaced nanoflake-assembled flower-like hierarchical ZnO microspheres prepared by bisolvents and their sensing properties to ethanol, J. Alloys Compd. 632 (2015) 645–650.
[28] A. Sinhamahapatra, A.K. Giri, P. Pal, S.K. Pahari, H.C. Bajaj, A.B. Panda, A rapid and green synthetic approach for hierarchically assembled porous ZnO nanoflakes with enhanced catalytic activity, J. Mater. Chem. 22 (2012) 17227.
[29] P. Kowalik, M. Konkol, K. Antoniak-Jurak, W. Próchniak, P. Wiercioch, M. Rawski, T. Borowiecki, Structure and morphology transformation of ZnO by carbonation and thermal treatment, Mater. Res. Bull. 65 (2015) 149–156.
[30] A. Hernández-Gordillo, F. Tzompantzi, R. Gómez, An efficient ZnS-UV photocatalysts generated in situ from ZnS(en)0.5 hybrid during the H2 production in methanol–water solution, Int. J. Hydrogen Energy 37 (2012) 17002–17008.
[31] R. Wahab, S.G. Ansari, Y.S. Kim, M.A. Dar, H.-S. Shin, Synthesis and characterization of hydrozincite and its conversion into zinc oxide nanoparticles, J. Alloys Compd. 461 (2008) 66–71.
[32] G. Mendoza-Damián, F. Tzompantzi, A. Mantilla, R. Pérez-Hernández, A. Hernández-Gordillo, Improved photocatalytic activity of SnO2-ZnAl LDH prepared by one step Sn4+ incorporation, Appl. Clay Sci. 121–122 (2016) 127–136.
[33] R.A.S. Safa, R. Hejazi, M. Rabbani, ZnO hierarchical nanostructures as a powerful photocatalyst ZnO hierarchical nanostructures as a powerful photocatalyst, Chin. J. Phys. 52 (2014) 1612–1624.
[34] L. Wang, J. Dai, X. Liu, Z. Zhu, X. Huang, P. Wu, Morphology-controlling synthesis of ZnS through a hydrothermal/solvthermal method, Ceram. Int. 38 (2012) 1873–1878.
[35] S. Kakarndee, S. Juabrum, S. Nanan, Low temperature synthesis, characterization and photoluminescence study of plate-like ZnS, Mater. Lett. 164 (2016) 198–201.
[36] A.A.P. Mansur, H.S. Mansur, F.P. Ramanery, L.C. Oliveira, P.P. Souza, Green colloidal ZnS quantum dots/chitosan nano-photocatalysts for advanced oxidation processes: study of the photodegradation of organic dye pollutants, Appl. Catal. B: Environ. 158–159 (2014) 269–279.